



Non-invasive Thermohydrodynamic Approach for Fast Cell Manipulation at the Microscale

Víctor de la Asunción-Nadal¹ · Marta Pacheco¹ · Beatriz Jurado-Sánchez^{1,2} · Estela Lapeira³ · Maialen Aginagalde³ · M. Mounir Bou-Ali³ · Alberto Escarpa^{1,2}

Received: 15 November 2023 / Revised: 5 February 2024 / Accepted: 15 February 2024
© The Author(s) 2024

Abstract

Thermal gradients have emerged as a promising technique for manipulating and sorting biological material at the microscale, holding considerable potential in lab-on-a-chip technology. Herein, we propose a non-invasive thermohydrodynamic approach for fast cell manipulation using a microfluidic open-to-air device. Cell discrimination is achieved by simply changing the temperature gradient toward the control of the convective effect on their displacement. First, the size and morphology/roughness-based motion capabilities were modeled using polystyrene (PS) microparticles with different sizes (5 and 20 μm) and polycaprolactone (PCL) microspheres, respectively. Computational fluid dynamics simulations of the generated flow were also carried out to demonstrate the influence of both the thermohydrodynamic and Marangoni effects in the PS particle displacement, where the thermally induced convective effect was not enough to move the microparticles inside the channel, but the combination of thermally induced convection together with the Marangoni effect. Indeed, small particles (5 μm) followed a full convective path, whereas the bigger ones (20 μm) exhibited a rolling motion on the substrate from the cold side to the hot side. Also, the relationship between in-flow speed and PCL ($\approx 20 \mu\text{m}$) surface roughness confirmed the driving force of this convection-based approach. Then, the microfluidic device was successfully used to separate Henrietta Lacks cancer cells (HeLa) from red blood (RBCs) and fibroblast (HFF-1) cells. To this end, thermal gradients were tailored to achieve the desired thermohydrodynamic effect, showing a highly versatile performance. Both cell models (HeLa-RBCs and HeLa-HFF-1), due to rationale tweaking of the imposed temperature gradients ($\Delta T = 10 \text{ K}$, 303–293 K, and $\Delta T = 5 \text{ K}$, 303–298 K), were efficiently separated in less than 5 and 60 s, respectively; with excellent cell viabilities. The proposed microfluidic approach holds considerable promise for thermohydrodynamic sorting and manipulation of biological material by non-invasive methods using portable instrumentation. The potential parallelization of the thermal-convective approach opens new avenues for early disease diagnosis (liquid biopsies) or the study of biological systems, even at physiological temperatures with a potential impact in cell (organ)-on-a-chip technologies.

Keywords Thermohydrodynamic convection · Marangoni effect · Microfluidics · RBCs · HeLa · Fibroblast cells

Víctor de la Asunción-Nadal and Marta Pacheco have contributed equally.

✉ M. Mounir Bou-Ali
mbouali@mondragon.edu

✉ Alberto Escarpa
alberto.escarpa@uah.es

¹ Department of Analytical Chemistry, Physical Chemistry and Chemical Engineering, University of Alcalá, 28802, Alcalá de Henares, Spain

² Chemical Research Institute “Andrés M. del Río”, University of Alcalá, 28802 Alcalá de Henares, Madrid, Spain

³ Department of Mechanical and Industrial Manufacturing, Mondragon Unibertsitatea, Mondragon Goi Eskola Politeknikoa, 20500 Mondragon, Spain

1 Introduction

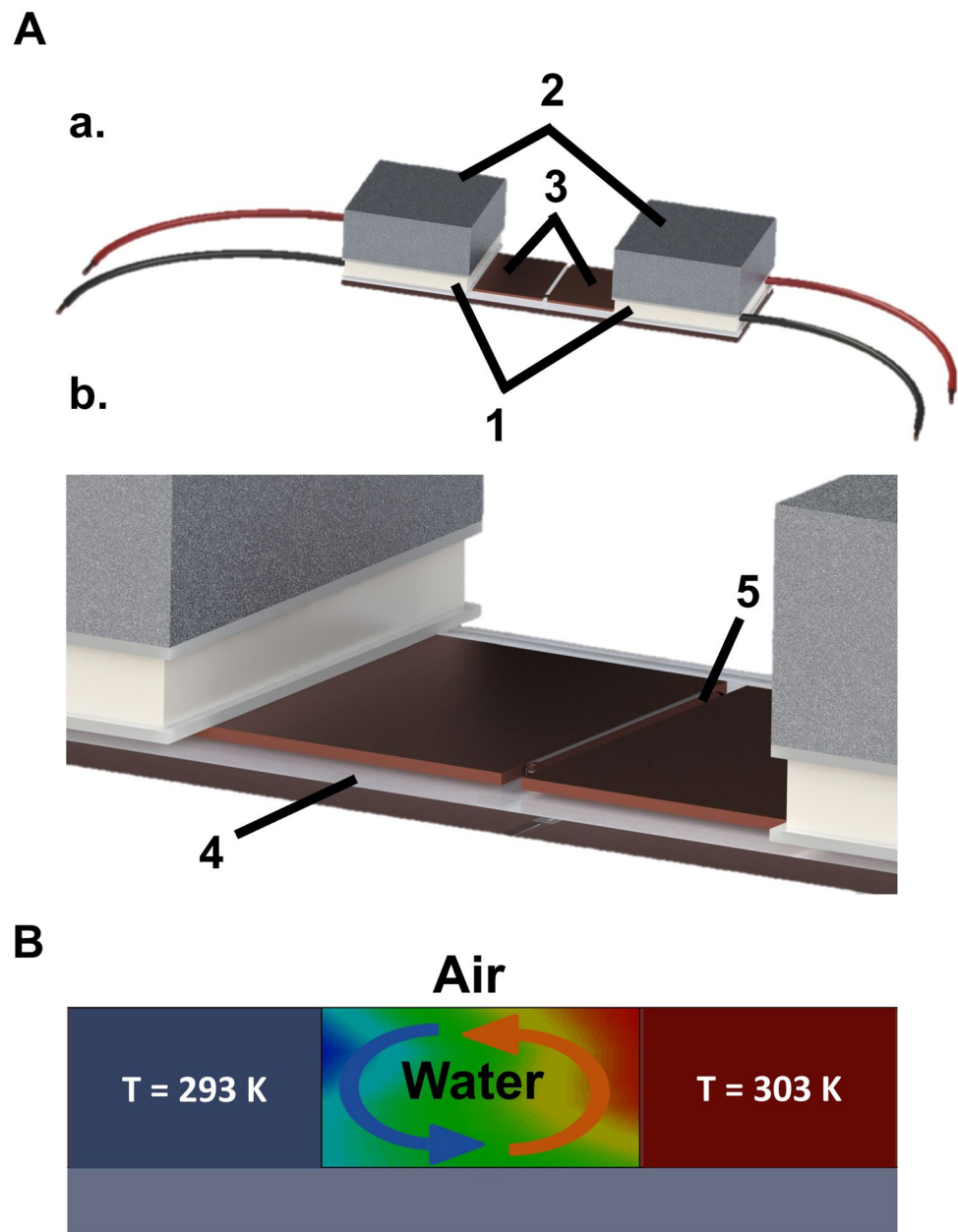
The controlled manipulation, trapping, and sorting of biological cells at the microscale is of paramount significance for early disease diagnosis or to study of biological systems and processes [1, 2]. To this end, different manipulation approaches have been reported, including microfluidics [3–5], optical [6], electrical [7, 8], thermal [9, 10], acoustic [3, 4], magnetic [11, 12] or chemical forces [13]. A myriad of applications including cell sorting [14], diagnosis, and cell characterization [15] have been achieved. Among the different methods for cell manipulation, the use of thermal gradients is particularly attractive due to its non-destructive

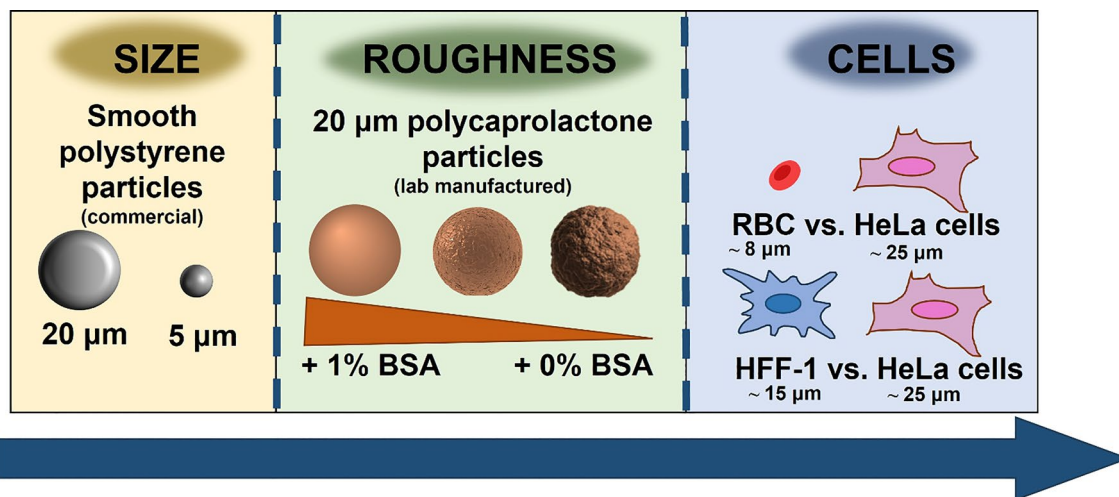
nature and the capabilities to keep the cells unaltered [16–18]. Indeed, thermodiffusion and thermohydrodynamics phenomena allow precise particle displacement, separation, and manipulation in microchannels [19] or the separation of toxic solvents from cryo-preserved cells [20].

Temperature gradients can be easily generated using microfluidic devices; allowing for the separation of suspended particles in fluids; which are driven selectively into warm or cold regimes [21–23]. The degree of separation is influenced by several variables such as temperature, particle size, roughness, hydrodynamical size, or salt concentration in the media. Such parameters can be easily tailored to achieve the separation of biological cells for

further diagnosis applications [21, 22, 24]. For example, the separation of DNA has been achieved in microchannels by light-induced local heating of the liquids inside the channels [21]. A thermophoretic device consisting of a silicon microchannel coupled with a heater has been used for the separation of microparticles from the driving fluid. The device generates a temperature gradient on both sides of the microchannel, requiring a difference of 1.5 K between the walls for efficient separation [25]. A polydimethylsiloxane (PDMS) microfluidic device with an integrated cover glass has been used for the thermophoretic separation of microspheres in salt-rich media. In this case, the thermal control was achieved by the circulation of water or by ohmic heating

Fig. 1 **A** Schematic of the thermal convection-based microfluidic device. The main components are labeled as follows: **a.1** thermoelectric heating/cooling elements (Peltier modules), **a.2** heat-dissipating aluminum blocks, **a.3** heat-conducting copper plates, **b.4** transparent glass substrate, **b.5** thermal-diffusive open air microfluidic channel (sample container). **B** Schematic of the generated mass transfer inside the open-to-air microfluidic channel due to the applied temperature gradient





Scheme 1 Conceptual route: the micro-objects and cells are chronologically studied to evaluate the motion’s capabilities driven by the thermo-hydrodynamic mechanism

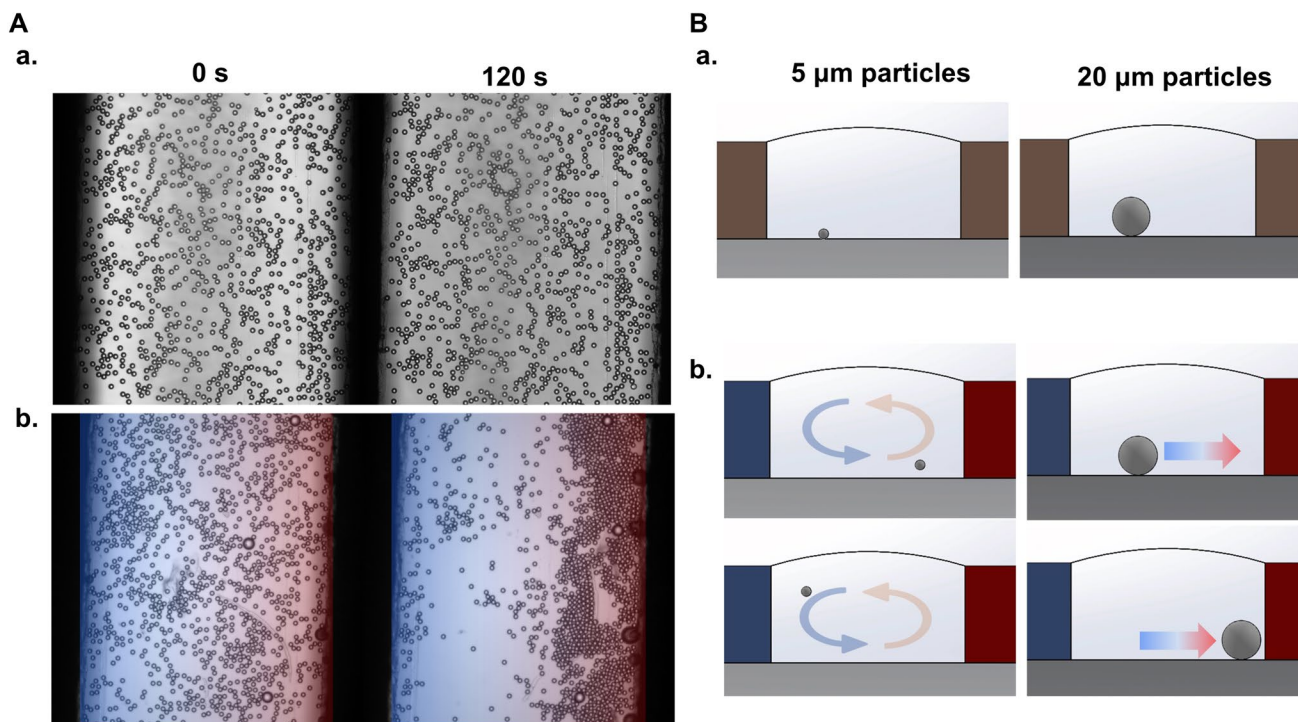


Fig. 2 **A** Time-lapse images (see Video S1) of standard 20 μm PS particles in water solution **a** without applying any temperature gradient and **b** under a 303 K (right wall) to 293 K (left wall) temperature gradient ($\Delta T = 10$ K). **B** Schematic depiction of the different behavior

of heavy 20 μm PS particles compared to that of lighter 5 μm particles (not to scale) **a** without applying any temperature gradient and **b** after applying a temperature gradient

of a channel adjacent to the test channel. The hot and cold thermal sources are placed on both sides of the microchip [26]. All the above-mentioned strategies have been applied for the separation of inert particles, as the operational temperature can denature cells. In this context, only early reports

demonstrated the utility of thermal field-flow fractionation and temperature gradients for the separation of bacteria cells, where the shape of similar-sized bacteria plays a critical role in the separation [27, 28]. Numerical simulations have illustrated the utility of a thermal convective-based

microfluidic chip with a non-continuous heat source for the separation of white blood cells from circulating tumor cells (CTCs). The principle of separation is based on the migration of white blood cells to the cold side of the microfluidic channel and the CTCs remain in the solution. While promising, the practical applicability has not been proven yet [29].

Herein, we will describe a thermohydrodynamic convection non-invasive approach based on an open-air microfluidic device for the discrimination of single cells that can be easily operated by non-specialized personnel. The device

consisted of two Peltier cells connected by two heat-conducting 500 μm copper plates separated 1 mm from each other. These copper plates will act as the walls of the thermohydrodynamic microchannel. As the microfluidic channel is open to the air, surface tension in the water–air interface needs to be taken into consideration. This creates a combination of thermohydrodynamic convection with the Marangoni effect when a temperature gradient is established. By tuning the applied voltage and the direction of the current, the generated gradient can be modulated to the desired

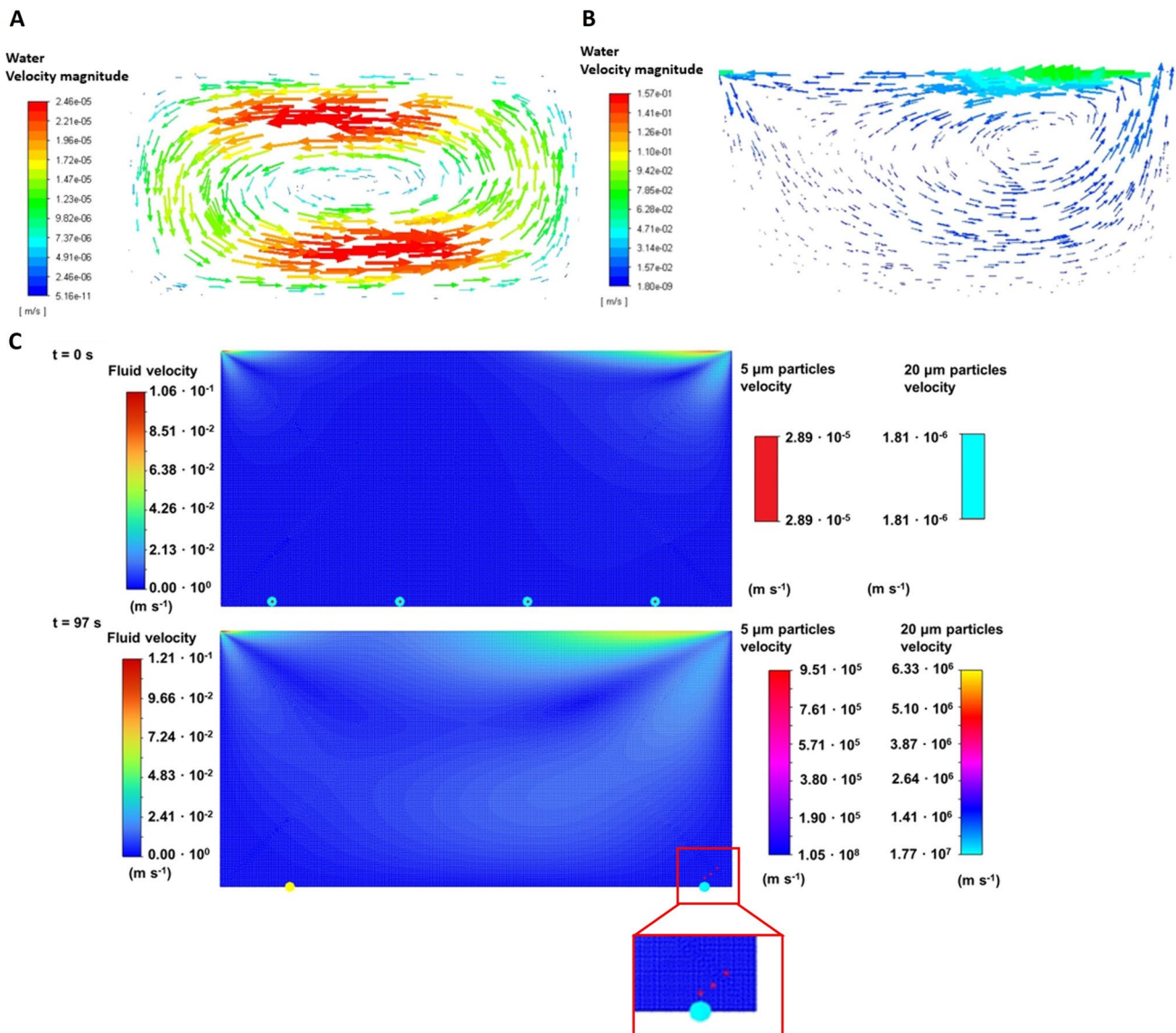


Fig. 3 Averaged stationary state velocities at the given conditions being the water–air interface. **A** Adiabatic wall, and **B** Water–air interface in the top part considering the interface surface tension in the function of the applied temperature gradient ($-0.0002 \text{ N m}^{-1} \text{ K}^{-1}$). **C** This image represents the movement capacity of particles of different sizes. Once the Marangoni convection is generated, all the 5 μm particles (represented in red) continue to move follow-

ing the convection current (as can be seen in the zoom). However, the 20 μm particles (represented in blue) move only towards the hot zone and remain there at the bottom of the channel. The left scale bar represents the fluid velocity magnitude and the ones that are in the right part represent the 5 μm particle velocity and 20 μm particle velocity are represented, respectively

temperatures. We will characterize first the movement of microparticles with different sizes to establish the principles behind this phenomenon using PS particles as a model. We will also study the influence of surface roughness on particle separation using PCL microspheres with different surface modifications. Once all these parameters are properly characterized, we will compare the motion characteristics of different cell types such as HeLa (cancerous cells), RBC (red blood cells), and HFF-1 (normal cells). We will illustrate the non-invasive label-free discrimination of HeLa directly from RBC due to their hydrodynamic characteristics. Additionally, the identification of similarly sized cell lines such as HeLa and HFF-1 cells will be also explored. The combination of thermal convection with the Marangoni effect based on an open-air microfluidic chip allows for a fairly easy operation and manipulation, as it only needs a fixed low voltage to establish the desired thermal gradient. To avoid hyperthermia-triggered cell death in the microfluidic channel, the applied temperature was limited to 303 K. The findings obtained with the proposed microfluidic system and the related numerical studies are relevant for future applications such as routine cell screening or pave the way for novel low-cost protocols for single-cell thermohydrodynamic characterization.

2 Materials and Methods

2.1 Reagents

PS microparticles (5 and 20 μm , cat. 79,633 and 74,491, respectively), bovine serum albumin (B8667), PCL (cat. 440,752), and sodium dodecyl sulfate (SDS, cat. 71,727) were obtained from Merck (Madrid, Spain). HeLa and HFF-1 cells were harvested at a confluency of 80%, using 10,000 cells in 24-well plates with 500 μL of culture media. PCL microparticles were synthesized by vigorous mixing, during 10 min, of 9 mL of 1% (w/v) of SDS with 1 mL of a chloroform solution containing 100 mg of PCL. The solution was dropped in a Petri dish overnight to promote particle generation. For surface modification with BSA, 10 μL of the PCL microsphere solution were incubated with 100 μL of a BSA solution (w/v) (0.01%, 0.1%, and 1%) for 90 min at 980 rpm and 298 K. All experiments involving cells were performed in *Centro de Apoyo a la Investigación en Medicina/Biología, Unidad de Cultivos Celulares* by authorized personnel and followed the University of Alcalá regulations. Rabbit blood samples treated with heparin were freshly obtained from *Centro de Experimentación Animal* of the University of Alcalá, following the official regulations. For RBC isolation, 2 mL of blood samples were centrifugated at 3000 rpm for 10 min. Then RBCs were washed five times with PBS solution for 10 min at 3000 rpm.

2.2 Instrumentation

The thermal convection-based device was designed at Mondragon University labs and assembled using a glass slide where two copper 500 μm thick plates were mounted. These plates were separated by a 1 mm distance and equipped with two Peltier elements (see Fig. 1) connected to an external power supply. By adjusting the magnitude and direction of the applied voltage, different temperatures can be obtained to generate the desired gradient. The temperature in the microfluidic device was determined, verified, and controlled by using a thermocouple during the experimental tests. Two aluminum cubes were used as a heat-dissipating element to minimize Joule heating. The sample can be placed directly in the open channel between the copper plates. Due to this open design, the glass slide can be easily washed between experiments. A thermocouple is used to determine and verify the temperatures on each side during experimental tests. To visualize the movement of the particles or cells, the device is placed directly on the sample holder of a Nikon Eclipse Instrument Inc. TiS/L100, coupled with 20X and 40X objectives, and a Zyla CMOS digital camera and NIS Elements AR 3.2 software. In normal operation conditions, the sample was introduced into the microfluidic chamber and allowed to settle. Thereafter, once all the cells or particles are settled at the bottom the predefined temperature gradient was established. Movies are captured at 25 frames per second and the movement (in terms of speed) of particles and cells is tracked using a NIS Elements tracking module. To ascertain the cleanliness of the microfluidic channel, the device was thoroughly cleaned with MilliQ water and ethanol. Once the device was properly cleaned and dried, the cleanliness of the microfluidic channel was checked in the optical microscope before the introduction of the samples.

An ASAP 2420–4 (Micromeritics) volumetric adsorption analyzer was used to determine BET surface areas and BJH pore size distributions of PCL nanoparticles, using nitrogen for adsorption and desorption at 77 K. The surface areas were calculated in the relative pressure range (P/P^0) from 0.05 to 0.20.

2.3 Cellular viability assay

The cell viability of HeLa and HFF-1 cells at the different experimentally tested temperatures was determined by MTT (3-[4,5-dimethylthiazol-2-yl]-2,5-diphenyl tetrazolium bromide) assay (Cell Proliferation Kit I, MTT, Roche, Germany). Cells were harvested at 80% confluency and plated in 24-well plates at 8,000 cells per well in 500 μL of media, using one plate for each experimental temperature condition. Next, the plates were incubated for 15 min, at 293 K, 298 K, 303 K, and 310 K as a control. After this time, 50 μL (5 mg mL^{-1}) MTT labeling reagents were added. Next,

the plate was incubated for 4 h in a humidified atmosphere (310 K (37 °C), 5% CO₂), and subsequently, 500 µl of the solubilization solution (DMSO) was added. The conversion of MTT into formazan by metabolically active cells indicated cell viability. The absorbance was measured at 570/630 nm using a microplate reader (Biotech Instrument) for the quantification of cell viability.

3 Results and Discussion

3.1 The Thermohydrodynamic Phenomena: PS Microparticle Size-Based Motion on a Microfluidic Device and Its Numerical Simulations

Figure 1A illustrates the schematic of the thermal convection-based microfluidic device (for more details see experimental section). The device is a miniaturized set-up, adopting a simple system configuration that can be easily operated. The main components are two Peltier cells physically connected to two heat-conducting 500 µm thick copper plates separated 1 mm from each other. These copper plates will act here as the walls of the thermal convective microfluidic channel. By tuning the applied voltage and the direction of the current, the generated gradient can be modulated to the desired temperatures. One of the Peltier cells is oriented with the hot side towards the copper plate, heating the copper plate to 303 ± 1 K while the other Peltier cell's orientation is inverted, cooling the second copper plate to 293 ± 4 K. This temperature gradient inside the open to air microfluidic channel forms a thermally induced convective current within the fluid body together with a Marangoni effect by having the upper part open to air as can be seen in Fig. 1B. This approach allows the control of the particle

separation-discrimination efficiency by simply changing the temperature gradient. That is, in a channel of a certain length, a higher temperature gradient causes a greater convective effect, increasing the displacement of particles. By applying smaller gradients (less convective effect), the average velocity is smaller, maximizing the particle–substrate interactions to discriminate between the particles.

The motion capabilities were explored using different micro-sized objects with different sizes, geometry, and surface properties, previously to cell assay (see scheme 1). As can be seen, a logical conceptual route was followed, from synthetic-based (PS-PCL microspheres) to biological systems (cells).

3.1.1 PS Microparticle Size-Based Experimental Assays

First, commercial 20 µm smooth PS particles in water were used. Yet, in the absence of a temperature gradient, no apparent particle separation is observed during gradient application (Fig. 2A, a) while as it is seen in Fig. 2A, b, (see also video S1) the 20 µm PS particles showcased a clear mean displacement to the hot side within a lapse of 120 s (particle enrichment), illustrating the crucial role of the thermally induced convective effect in the motion of microsized PS particles.

Then to evaluate the influence of particle size on the convective motion, smooth PS particles of 5 µm were also studied and then compared with the 20 µm microparticle motion. As can also be seen in Video S1, the differentiated motion recorded reveals the influence of the size on microparticle separation. Figure 2B shows the schematic depiction of the different microparticle size behavior observed. While, the 5 µm particles were small enough to be lifted by the hot upward stream and travel back to the cold side in a higher plane (see left scheme on Fig. 2B, a) by the convection generated inside the channel, the bigger 20 µm particles, result in a directed movement from the cold side to the hot side followed by accumulation on the hot wall (see right scheme on Fig. 2B, b). Stoke numbers of both particles are smaller than 1, therefore they follow the streamlines of the convection current. However, we can observe that the small particles can follow the full convective path, whereas the bigger particles are only able to exhibit a rolling motion on the substrate from the cold side to the hot side. Indeed, this differentiated behavior may be due to the weight of bigger particles that compared to the small ones the gravitational field overlaps the convective regime. Thus, in the case of 20 µm particles a downward net force is established, not allowing bigger particles to travel upwards and backward in the upper backflow.

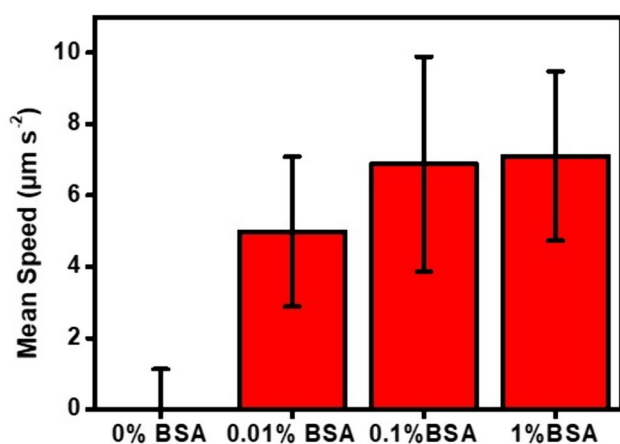


Fig. 4 Mean speeds of unmodified and modified with different concentrations of BSA PCL microparticles (see Video S2)

3.1.2 Numerical Simulations

To further understand the processes involved in the thermohydrodynamic motion of the microparticles, a series of numerical simulations were performed. To this end, the Ansys fluent2021 R1 software was employed. For all the numerical studies, a rectangular 0.5 mm × 1 mm cavity was simulated, using water as a model fluid, and considering laminar flow only. For all the simulations the temperature gradient was set at 10 K, from 293.15 to 303.15 K. The substrate was simulated as an adiabatic wall in all cases, whereas the water–air boundary was simulated differently to validate the model before analyzing particle migration inside the channel: as an adiabatic wall (Fig. 3A) and considering the boundary condition for the water–air surface tension in the function of the temperature with a value equal -0.0002 N m⁻¹ K⁻¹ (Fig. 3B) [30].

The mathematical model formulation of mass, momentum, and energy conservation laws were defined as Eq. (1), (2) and (3) respectively,

$$\nabla \cdot \vec{u} = 0 \tag{1}$$

$$(\vec{u} \cdot \nabla)\vec{u} = -\frac{1}{\rho}\nabla p + \nabla \cdot (v\nabla\vec{u}) \tag{2}$$

$$\nabla \cdot (\vec{u}c_p T) = \nabla \cdot \left(\frac{k}{\rho}\nabla T\right) \tag{3}$$

where ρ is the liquid’s density, \vec{u} is the velocity, v represents the kinematic viscosity, c_p correspond to the specific heat and k the thermal conductivity. P and T refer to the liquid’s pressure and temperature, respectively.

All the simulations we have carried out with a quadrilateral 2D mesh with an element size of 2×10^{-6} m, average skewness of 1.44×10^{-2} , average element quality of 0.97, and applying and inflation of 4 layers near boundaries to improve the accuracy.

From the results, we can assume that the mass transport process within the microfluidic channel in Fig. 3B is driven by the combination of the thermally induced convection together with the Marangoni effect. Specifically, the convection generated due to the Marangoni effect has the dominant contribution as can be seen in the velocity magnitude which is 1000 times bigger compared to the case of Fig. 3A. In these working conditions, the Marangoni number is 1.54×10^4 according to the Eq. (4),

$$Ma = -\frac{\partial\sigma}{\partial T} \frac{L_c \Delta T}{\mu\alpha} \tag{4}$$

where, $\frac{\partial\sigma}{\partial T}$ is the surface tension variation in function of temperature (N/mK), L_c is the characteristic length (m), ΔT is

the temperature difference (K), μ is the fluid dynamic viscosity (Pa · s) considering 9×10^{-4} for water at 25°C and α is the thermal diffusivity of the liquid (m²/s) considering 1.44×10^{-7} for water at 25°C.

Once the base fluid model was validated, the particle track inside the channel was analyzed considering the fluid condition as in Fig. 3B, which is the case of the experimental device. For the particle tracking the Discrete Phase Model (DPM) was used by selecting Thermophoretic Force as a physical model as can be seen in the Eq. (5),

$$\frac{d\vec{u}_{particle}}{dt} = \frac{18\mu C_D R_e}{\rho_p d_p^2 24} (\vec{u} - \vec{u}_{particle}) + \frac{\vec{g}(\rho_{particle} - \rho)}{\rho_{particle}} + \vec{F}_T \tag{5}$$

Considering $\left(\left(\frac{18\mu C_D R_e}{\rho_p d_p^2 24}\right) \cdot (\vec{u} - \vec{u}_{particle})\right)$ as the spherical particles drag force per unit mass, where C_D is the drag coefficient and $\left(R_e \equiv \rho d_p \left|\vec{u}_p - \vec{u}\right| / \mu\right)$ is the relative Reynolds number. $\left(\vec{F}_T\right)$, is the additional acceleration (force per unit mass) due to the thermophoretic effect and was defined as Eq. (6).

$$\vec{F}_T = -D_{T,fluent} \frac{1}{m_{p,i}} \frac{\partial T}{\partial x} \tag{6}$$

where, $m_{p,i}$ is the corresponding mass of the particle i , and $D'_{T,fluent}$ is the thermophoresis coefficient. This coefficient is defined in Ansys Fluent by Tablot’s expression for gases, but for liquids, we have based on [31] works with the following Eq. (7).

$$D'_{T,fluent} = 6\pi\mu R_{particle,i} T D'_{T,i} \tag{7}$$

where μ (Pa · s) is the dynamic viscosity of the base fluid, $R_{particle,i}$ is the radius of the particle, T is the temperature of the base fluid and $D'_{T,i}$ (m²/s · K) is the thermodiffusion coefficient of the PS particles [32].

According to numerical simulation results (Fig. 3C), the thermally induced convective effect is not enough to move the microparticles inside the channel, as already demonstrated in previous works [31]. Otherwise, the combination of thermally induced convection together with the Marangoni effect, which is the case of the experimental device, shows that both 5 μm and 20 μm particles migrate to the hot zone (Fig. 3C). According to transient numerical simulations and experimental tests, it is possible to appreciate that particles of 5 μm migrate to the hot zone and after being lifted to the top part, they are dragged to the cold side again generating a convective-like path (Fig. 3C, red particles). On the contrary, in the case of 20 μm particles, it is noticeable that particles migrate to the hot side, but the flow is not able to lift them (Fig. 3C, blue particles). In other words, at the initial state (Fig. 3C top) all particles are distributed across the

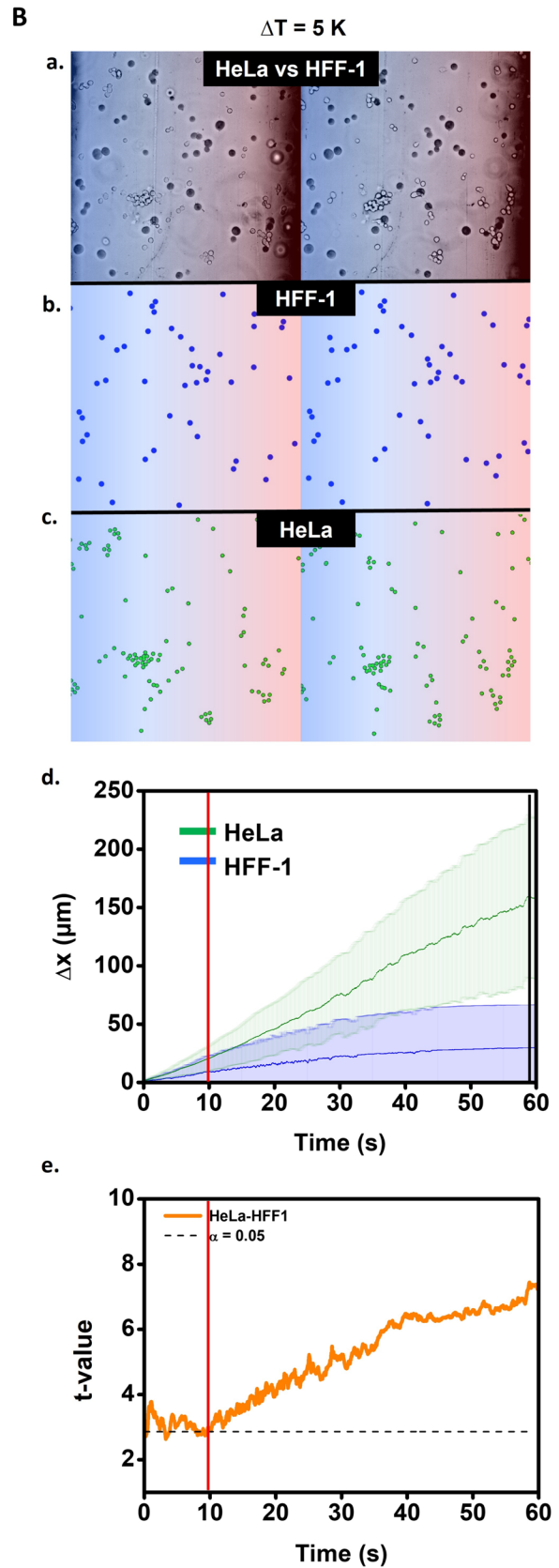
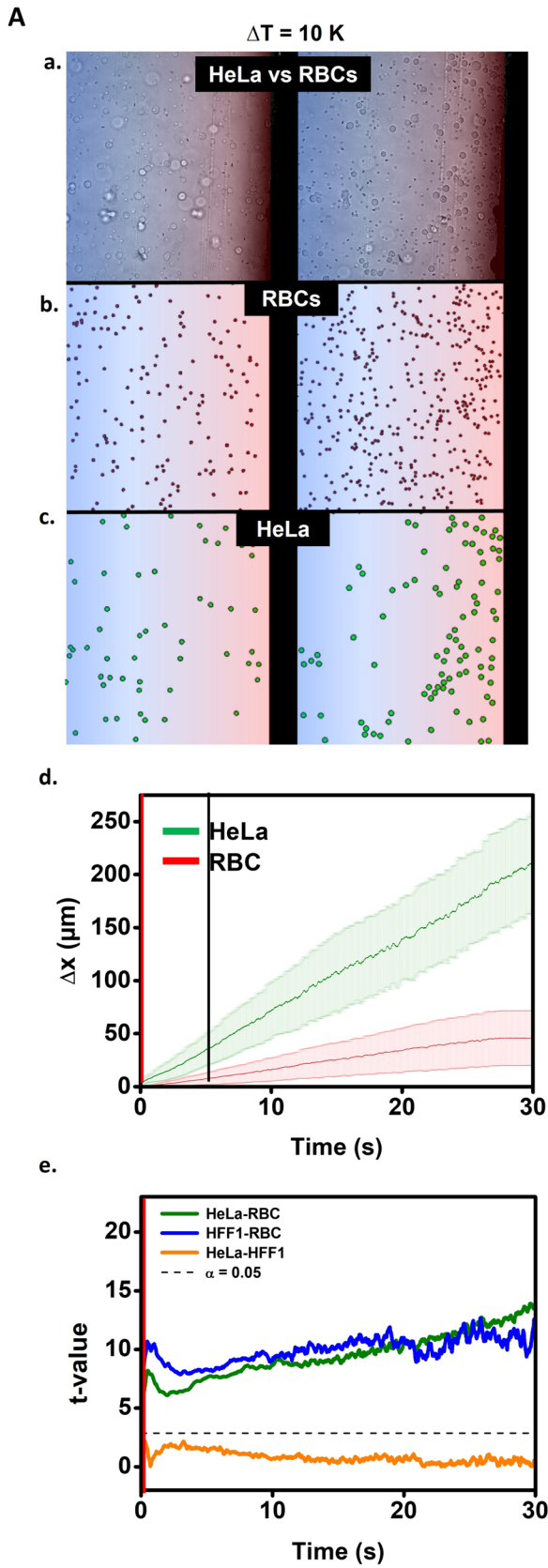


Fig. 5 **A** HeLa cell discrimination from RBCs in the blood, and **B** HeLa cell discrimination from the HFF-1 cell line, using the thermal convection-based device. Images of cell mixtures prior (left) and after a 60-s treatment (right) (see Video S3): **a** Bright-field images of RBC-HeLa mixture (**A**) and superimposed HeLa and HFF-1 (**B**), **b**, **c** RBC (red), HeLa (green), and HFF-1 (blue) cell population maps. **d** Cell position differentials along the x-axis and statistical deviation of 20 red blood cells (red), 20 HeLa cells (green), and 20 HFF-1 cells (blue). Note that the vertical black solid lines indicate visual cellular separation, and the red solid lines indicate statistically significant separation. **e** Time-dependent p-values for each cell line pair: HeLa & RBC (green), HFF-1 & RBCs (blue), and HeLa & HFF-1 (orange); and cut-off value for a 95% confidence level. Note that in **A**), the thermal gradient was set at $\Delta T = 10$ K (303–293K), whereas in **B**), the thermal gradient was set at $\Delta T = 5$ K (303–298K)

width of the channel. In equilibrium state (Fig. 3C bottom) 5 μm particles continue moving in the x direction (toward the hot zone) and lifting in the channel (following the convection current). In contrast, 20 μm particles move in the x direction (toward the hot zone); however, when they reach the hot wall, they start decelerating and are not able to lift.

3.2 The Thermohydrodynamic Phenomena: Influence of Roughness on Microparticle Separation

While the study discussed above demonstrates the movement ability of microparticles with different sizes, conceptually following Scheme 1, the influence of the shape and surface roughness as a hydrodynamic variable was also evaluated using 20 μm unmodified PCL microparticles, a mesoporous material with a large specific surface area and porosity [33, 34]. The PCL microparticles were synthesized using an emulsion technique (see experimental section). Subsequently, to decrease the surface roughness, and study the effect on surface modification, the PCL microparticles were modified by incubation with different concentrations of bovine serum albumin (BSA) [35]. The roughness decreased upon the increase in the BSA concentration, as illustrated by BET studies. Indeed, the mean surface of unmodified PCL particles is 25% larger than that of 1% BSA-modified PCL microparticles (1.74 m^2/g compared to 1.31 m^2/g , respectively). The particles were introduced in the open channel to analyze the transport mechanism under the 303 K to 293 K temperature gradient (same gradient $\Delta T = 10$ K, see Video S2). Videos were recorded as specified in the experimental section and the overall root mean square speed was calculated (see Fig. 4). The PCL microparticles eventually reach their maximum velocity at a BSA concentration near 1%, whereas unmodified particles show negligible motion. This fact demonstrates the relationship between in-flow speed and surface roughness and shows the discrimination based on the

thermohydrodynamic and Marangoni convection movement of microparticles with different surface modifications.

3.3 The Thermohydrodynamic Phenomena: Cell Discrimination

The main advantage of the thermal convection-based device described here is the ability to propel objects in the micro-scale in a controlled and non-invasive way. Indeed, properties such as size and roughness had a significant influence on the microparticles' motion. Also, since the performance was evaluated under mild thermal conditions, it is feasible to apply this concept to cell systems.

To this end, we tested the displacement of different cells such as an adenocarcinoma cell line (HeLa cells, ~ 25 μm , rounded shape) and RBC (~ 8 μm , rounded shape like a biconcave disc, with a central depression) under mild conditions taking in advantage the morphological and size differences. The results are shown in Fig. 5. Optical microscopy images of a HeLa and diluted blood cell mixtures were taken before ($t = 0$ s) applying the specified temperature gradient (303–293 K, $\Delta T = 10$ K), and after 60 s of thermal treatment (see, Fig. 5a–c, Video S3). These images were transformed into binary black and white maps and the images were analyzed using the ImageJ software automatic particle counting and particle analysis module. Hence, 20 cells of each type were tracked, and the mean displacement and statistical deviation were plotted. As can be seen in Fig. 5A, d, the mean displacement of RBC and HeLa cells were visually rapidly different in just 5 s (see black solid line in Fig. 5A, d), demonstrating the differentiated thermohydrodynamic features of both cell types. According to the mean displacement results, bigger rounder HeLa cells show higher speeds when compared to flatter RBCs. This observation might be due to the different morphologies, as round cells can “roll” along the surface of the substrate (Eq. 5). On the other hand, RBCs present stronger cell-substrate interactions due to their higher surface/volume ratio and the lack of available rotation symmetry operations parallel to the substrate.

The thermohydrodynamic capabilities of adenocarcinoma cells (HeLa, ~ 25 μm), and human fibroblasts (HFF-1, ~ 15 μm) were further explored taking in advance the superficial differences in the outer membrane (roughness), and mechanical properties (stiffness) of differentiated cells. However, as seen in Fig. 5A, e, the separation of HeLa and HFF-1 cells was unsuccessful when applying a temperature gradient of 10 K. This lack of separation was attributed to the short gradient time applied due to the fast convection in the channel. To allow the identification of both cell lines, the temperature was set to 298 K and 303 K in the cold and hot sides, respectively. So, the applied gradient was modified from 10 to 5 K to minimize the mean speed,

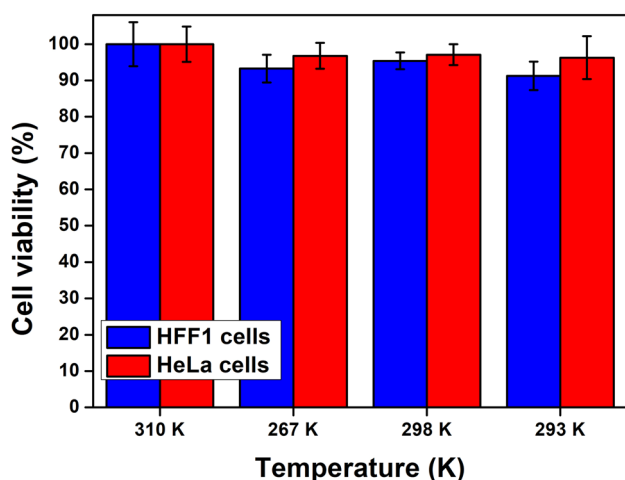


Fig. 6 Cellular viability MTT assay of HeLa and HFF-1 cells exposed at different temperatures after 15 min of incubation

thus maximizing the cell-substrate interaction and investing sufficient thermal gradient application time to discriminate the cell lines by exploiting the differentiated cell-substrate interaction strength due to their different morphologies. As can be seen in Fig. 5B, d, with a shorter temperature gradient, cells show lower mean velocities (Video S4) which exert an influence on the final displacement resulting in a total visual discrimination of both cellular systems once a thermal gradient application time has elapsed to 60 s (see black solid line in Fig. 5B, d). This confirms the thermohydrodynamic discriminatory capabilities on HeLa and HFF-1 cell lines within the purposed microfluidic system.

This claim is further supported by the results depicted in Fig. 5B, e. Here, a time-dependent t -test was performed for each data point ($n=20$) obtaining the corresponding t -value for each cell line pair at each time. The t -value for a significance level $\alpha=0.05$ was represented in the corresponding graph. As can be observed, at $\Delta T=10$ K a statistical difference between both HFF-1 and HeLa and RBC is noted from the beginning of the thermohydrodynamic operation ($\alpha>0.05$, $t=0$ s, see also red solid line in Fig. 5A, d). However, HFF-1 and HeLa (at $\Delta T=10$ K) showed similar behavior and cell separation was not achieved (see orange graph line in Fig. 5A, e). On the other hand, at $\Delta T=5$ K a statistical difference between HeLa and HFF-1 is noted after applying the thermal gradient for approximately 10 s (see red solid line in Fig. 5B, d). Please note the presence of immotile particles, both in HeLa and HFF-1 culture samples. To the statistical determination of the hydrodynamic features of such cell types, both non-hydrodynamic cells and cell clusters were not considered for further calculations.

Additionally, cell viability studies at the different applied temperatures (293 K, 298 K, 303 K, and 310 K as control) were performed using the HeLa and HFF-1 cell lines with

a colorimetric assay employing 3-(4,5-dimethylthiazol-2-yl)-2,5-diphenyltetrazolium bromide (MTT). As shown in Fig. 6, the temperatures applied in the microfluidic device are soft and non-invasive, obtaining cell viabilities close to 100% in all cases during 15 min of exposure (please, note that cell separation experiments were carried out for 60 s, much smaller times). Note that the objective of the thermal and Marangoni convection-based microfluidic device applied to biological material is a preliminary *in vitro* test that demonstrates the separation between cells with morphological differences with potential for (routine)-analysis in laboratories. In a real clinical scenario, the method illustrated here holds considerable promise for cell discrimination in a myriad of clinical and biological applications, especially in liquid biopsies. Our method is a versatile approach that allows the separation efficiency to be modulated by simply changing the temperature gradient to minimize the average velocity, thus maximizing the cell-substrate interaction to discriminate cell lines such as cancerous and normal cells or CTCs by exploiting the strength of differentiated cell-substrate interaction due to their different morphologies. The method is very cheap and can be easily implemented, even in a doctor's office, for fast sorting and classification of samples, avoiding the use of expensive flow cytometers or other devices. This is particularly attractive as well in low-resource countries.

4 Conclusions

A thermal and Marangoni convection-based microfluidic device has been successfully designed, modeled, and employed for ultra-fast cell visual separation and enrichment under mild conditions (low operational temperature gradient) to ensure high cell viability. Experimental studies and related simulations indicate the critical role of particle size and roughness for successful discrimination. The bigger and smoother particles experience an effective migration from the cold to the hot side of the device, smaller particles are dragged inside the convection flux, which is dominated by the Marangoni effect, whereas bigger ones result in a directed movement from the cold side to the hot side followed by accumulation on the hot wall and rougher particles are not able to overcome the drag forces, remaining unaltered.

More importantly, such tailored manipulation was successfully exploited to discriminate HeLa from RBCs and HFF-1 cells in less than 5 and 60 s visually, respectively; under-designed and controlled thermohydrodynamics using tailored thermal gradients showing a high versatility performance. Furthermore, cell viability tests showed that the applied thermal gradients in the microfluidic device are non-invasive and biologically safe in the given conditions.

Regardless, physiological temperatures could be used if needed, obtaining similar separation results by applying the same temperature gradients.

Key advantages of the thermohydrodynamic approach, compared to existing cell manipulation methods, are its low cost and ease of operation. Furthermore, the approach offers high separation efficiency and versatility. In addition, the visualization can be performed in situ without the need for cell-imaging reagents or sophisticated equipment toward a label-free approach. The operation of single-channel separation is demonstrated here as a proof of concept. However, more microchannels could be integrated to perform simultaneous and/or multiplexed cellular analysis, in addition to the incorporation of device input and output channels that allow flow analysis of samples and obtaining separate cellular fractions, owing to the inherent parallelization, and coupling to other characterization techniques.

All in all, the thermohydrodynamic-based microfluidic approach illustrated here holds considerable promise for cell manipulation (discrimination and isolation) in a myriad of clinical and biological applications, with special potential in cell (organ)-on-a-chip technology and in liquid biopsies to detect tumor cells (even detection of CTCs which remains a challenge to this date) in relevant samples allowing a fast cancer diagnosis and timely treatments to increase the survival rate of patients.

Supplementary Information The online version contains supplementary material available at <https://doi.org/10.1007/s13206-024-00145-3>.

Acknowledgements This work was supported by the Spanish Ministry of Science Innovation, Grant PID2020-118154GB-I00 funded by MCIN/AEI/<https://doi.org/10.13039/501100011033> (A. E and B.J.S) and the European Union “NextGenerationEU”/PRTR (A. E and B.J.S), Ministry of science and innovation [PID2020-115086GB-C33 to M.B.A], the Community of Madrid [grant numbers CM/JIN/2021-012 (B.J.S), and the Community of Madrid grant number Y2020/NMT6312 (NEURO-CHIP-CM) program (A.E.)] and the Basque Government [IT1505-22 and M4SMART (KK-2023/00016)].

Author Contributions Víctor de la Asunción-Nadal: Conceptualization, Data curation, Formal analysis, Investigation, Visualization, Writing-review & editing. Marta Pacheco: Conceptualization, Data curation, Formal analysis, Investigation, Visualization, Writing-review & editing. Beatriz Jurado-Sánchez: Formal analysis, Funding acquisition, Supervision, Writing-Original draft; Writing -review & editing. Estela Lapeira: Data curation, Formal analysis, Investigation, Writing-review & editing. Maialen Aguinagalde: Data curation, Investigation, Writing-review & editing. Mounir Bou-Ali: Conceptualization, Data curation, Funding acquisition, Project administration, Resources, Supervision, Writing -review & editing. Alberto Escarpa: Conceptualization, Data curation, Funding acquisition, Project administration, Resources, Supervision, Writing -review & editing.

Funding Open Access funding provided thanks to the CRUE-CSIC agreement with Springer Nature.

Declarations

Conflict of Interest The authors declare that they have no conflicts of interest.

Open Access This article is licensed under a Creative Commons Attribution 4.0 International License, which permits use, sharing, adaptation, distribution and reproduction in any medium or format, as long as you give appropriate credit to the original author(s) and the source, provide a link to the Creative Commons licence, and indicate if changes were made. The images or other third party material in this article are included in the article’s Creative Commons licence, unless indicated otherwise in a credit line to the material. If material is not included in the article’s Creative Commons licence and your intended use is not permitted by statutory regulation or exceeds the permitted use, you will need to obtain permission directly from the copyright holder. To view a copy of this licence, visit <http://creativecommons.org/licenses/by/4.0/>.

References

- Pang, Y., Song, H., Kim, J.H., Hou, X., Cheng, W.: Optical trapping of individual human immunodeficiency viruses in culture fluid reveals heterogeneity with single-molecule resolution. *Nat. Nanotechnol.* **9**, 624–630 (2014)
- Yun, H., Kim, K., Lee, W.G.: Cell manipulation in microfluidics. *Biofabrication* **5**, 022001 (2013)
- Petersson, F., Åberg, L., Swärd-Nilsson, A.M., Laurell, T.: Free flow acoustophoresis: microfluidic-based mode of particle and cell separation. *Anal. Chem.* **79**, 5117–5123 (2007)
- Zhou, Y., Ma, Z., Ai, Y.: Hybrid microfluidic sorting of rare cells based on high throughput inertial focusing and high accuracy acoustic manipulation. *RSC Adv.* **9**, 31186–31195 (2019)
- Wang, J., Ma, P., Kim, D.H., Liu, B.-F., Demirci, U.: Towards microfluidic-based exosome isolation and detection for tumor therapy. *Nano Today* **37**, 101066 (2021)
- Landenberger, B., Höfemann, H., Wadle, S., Rohrbach, A.: Microfluidic sorting of arbitrary cells with dynamic optical tweezers. *Lab Chip* **12**, 3177–3183 (2012)
- Mernier, G., Piacentini, N., Braschler, T., Demierre, N., Renaud, P.: Continuous-flow electrical lysis device with integrated control by dielectrophoretic cell sorting. *Lab Chip* **10**, 2077–2082 (2010)
- Shafiee, H., Caldwell, J.L., Sano, M.B., Davalos, R.V.: Contactless dielectrophoresis: a new technique for cell manipulation. *Biomed. Microdevices* **11**, 997 (2009)
- Somà, A., Iamoni, A., Voicu, R., Müller, R., Al-Zandi, M.H.M., Wang, C.: Design and experimental testing of an electro-thermal microgripper for cell manipulation. *Microsyst. Technol.* **24**, 1053–1060 (2018)
- Lin, L., Peng, X., Wei, X., Mao, Z., Xie, C., Zheng, Y.: Thermophoretic tweezers for low-power and versatile manipulation of biological cells. *ACS Nano* **11**, 3147–3154 (2017)
- Hultgren, A., Tanase, M., Chen, C.S., Meyer, G.J., Reich, D.H.: Cell manipulation using magnetic nanowires. *J. Appl. Phys.* **93**, 7554–7556 (2003)
- Liu, C., Stakenborg, T., Peeters, S., Lagae, L.: Cell manipulation with magnetic particles toward microfluidic cytometry. *J. Appl. Phys.* **105**, 102014 (2009)
- Shin, S.: Diffusiophoretic separation of colloids in microfluidic flows. *Phys. Fluids* **32**, 101302 (2020)

14. Wyatt Shields IV, C., Reyes, C.D., López, G.P.: Microfluidic cell sorting: a review of the advances in the separation of cells from debulking to rare cell isolation. *Lab Chip* **15**, 1230–1249 (2015)
15. Shukla, V.C., Kuang, T.-R., Senthilvelan, A., Higuaita-Castro, N., Duarte-Sanmiguel, S., Ghadiali, S.N., Gallego-Perez, D.: Lab-on-a-chip platforms for biophysical studies of cancer with single-cell resolution. *Trends Biotechnol.* **36**, 549–561 (2018)
16. Rahman, M.A., Saghir, M.Z.: Thermodiffusion or Soret effect: historical review. *Int. J. Heat Mass Transf.* **73**, 693–705 (2014)
17. Chen, J., Cong, H., Loo, F.-C., Kang, Z., Tang, M., Zhang, H., Wu, S.-Y., Kong, S.-K., Ho, H.-P.: Thermal gradient induced tweezers for the manipulation of particles and cells. *Sci. Rep.* **6**, 35814 (2016)
18. Jain, A., Goodson, K.E.: Thermal microdevices for biological and biomedical applications. *J. Therm. Biol.* **36**, 209–218 (2011)
19. Eslamian, M., Saghir, M.Z.: Novel thermophoretic particle separators: Numerical analysis and simulation. *Appl. Therm. Engineering* **59**, 527–534 (2013)
20. Martin-Mayor, A., Bou-Ali, M.M., Aginagalde, M., Urteaga, P.: Microfluidic separation processes using the thermodiffusion effect. *Int. J. Therm. Sci.* **124**, 279–287 (2018)
21. Thamdrup, L.H., Larsen, N.B., Kristensen, A.: Light-induced local heating for thermophoretic manipulation of DNA in polymer micro- and nanochannels. *Nano Lett.* **10**, 826–832 (2010)
22. Duhr, S., Braun, D.: Why molecules move along a temperature gradient. *Proc. Natl. Acad. Sci.* **103**, 19678–19682 (2006)
23. Helden, L., Eichhorn, R., Bechinger, C.: Direct measurement of thermophoretic forces. *Soft Matter* **11**, 2379–2386 (2015)
24. Errarte, A., Martin-Mayor, A., Aginagalde, M., Iloro, I., Gonzalez, E., Falcon-Perez, J.M., Elortza, F., Bou-Ali, M.M.: Thermophoresis as a technique for separation of nanoparticle species in microfluidic devices. *Int. J. Therm. Sci.* **156**, 106435 (2020)
25. Geelhoed, P.F., Lindken, R., Westerweel, J.: Thermophoretic separation in microfluidics. *Chem. Eng. Res. Des.* **84**, 370–373 (2006)
26. Vigolo, D., Rusconi, R., Stone, H.A., Piazza, R.: Thermophoresis: microfluidics characterization and separation. *Soft Matter* **6**, 3489–3493 (2010)
27. Janča, J., Halabalová, V., Růžička, J.: Role of the shape of various bacteria in their separation by Microthermal Field-Flow Fractionation. *J. Chromatogr. A* **1217**, 8062–8071 (2010)
28. Janča, J., Kašpárková, V., Halabalová, V., Šimek, L., Růžička, J., Barošová, E.: Micro-thermal field-flow fractionation of bacteria. *J. Chromatogr. B* **852**, 512–518 (2007)
29. Asiaei, S., Darvishi, V., Davari, M.H., Zohrevandi, D., Moghadasi, H.: Thermophoretic isolation of circulating tumor cells, numerical simulation and design of a microfluidic chip. *J. Therm. Anal. Calorim.* **137**, 831–839 (2019)
30. Vargaftik, N.B., Vinogradov, Y.K., Yargin, V.S.: *Handbook of Physical Properties of Liquids and Gases: New Augmented and Revised Edition of the Classic Reference.* Begell House (1996)
31. Sanjuan, A., Errarte, A., Bou-Ali, M.M.: Analysis of thermophoresis for separation of polystyrene microparticles in microfluidic devices. *Int. J. Heat Mass Transf.* **189**, 122690 (2022)
32. Braun, S.D.A.D.: Why molecules move along a temperature gradient. *Proc. Natl. Acad. Sci.* **103**, 19678–19682 (2006)
33. Huang, X., Gao, J., Li, W., Xue, H., Li, R.K.Y., Mai, Y.M.: Preparation of poly (ϵ -caprolactone) microspheres and fibers with controllable surface morphology. *Mater. Des.* **117**, 298–304 (2017)
34. Jurado-Sánchez, B., Pacheco, M., Rojo, J., Escarpa, A.: Magneto-catalytic graphene quantum dots Janus micromotors for bacterial endotoxin detection. *Angew. Chem. Int. Ed.* **56**, 6957–6961 (2017)
35. Liu, C., Guo, Y., Hong, Q., Rao, C., Zhang, H., Dong, Y., Huang, L., Lu, X., Bao, N.: Bovine serum albumin adsorption in mesoporous titanium dioxide: pore size and pore chemistry effect. *Langmuir* **32**, 3995–4003 (2016)

Publisher's Note Springer Nature remains neutral with regard to jurisdictional claims in published maps and institutional affiliations.